




Scaling of Dzyaloshinskii-Moriya interaction with magnetization in Pt/Co(Fe)B/Ir multilayers

Khulaif Alshammari ^{1,2}, Eloi Haltz,¹ Mohammed Alyami,^{1,3} Mannan Ali,¹ Paul S. Keatley,⁴ Christopher H. Marrows ¹, Joseph Barker,¹ and Thomas A. Moore ^{1,*}

¹*School of Physics and Astronomy, University of Leeds, Leeds LS2 9JT, United Kingdom*

²*Physics Department, College of Science, Jouf University, P.O. Box 2014, Sakaka 42421, Saudi Arabia*

³*Department of Physics, College of Science and Humanities in Al-Kharj, Prince Sattam bin Abdulaziz University, Al-Kharj 11942, Saudi Arabia*

⁴*Department of Physics and Astronomy, University of Exeter, Exeter EX4 4QL, United Kingdom*



(Received 19 August 2021; accepted 15 November 2021; published 1 December 2021)

Magnetic multilayers with perpendicular anisotropy and an interfacial Dzyaloshinskii-Moriya interaction (DMI) contain chiral domain walls and skyrmions that are promising for applications. Here, we measure the temperature dependence of the DMI in Pt/CoFeB/Ir and Pt/CoB/Ir multilayers by means of static domain imaging. First, the temperature dependences of saturation magnetization (M_S), exchange stiffness (A), and intrinsic perpendicular anisotropy (K_u) are determined. Then the demagnetized domain pattern in each multilayer is imaged by wide-field Kerr microscopy in the temperature range 9–290 K, and the characteristic domain period at each temperature is determined. We calculate the DMI constant D from an analytical expression for the domain wall energy density that treats the multilayer as a uniform medium. Scaling laws for K_u and D with the magnetization are established from the experiments. While the scaling of K_u is consistent with Callen-Callen theory, we find that the scaling of D is like that of A predicted theoretically (~ 1.8).

DOI: [10.1103/PhysRevB.104.224402](https://doi.org/10.1103/PhysRevB.104.224402)

I. INTRODUCTION

In magnetic multilayers, the interfacial Dzyaloshinskii-Moriya interaction (DMI) [1] causes domain walls to have a chiral spin structure, and if it exceeds a critical value, skyrmions can be stabilized [2]. Even larger values of DMI produce spin spirals. The different chiral spin textures are stable only in quite limited regions of a parameter space where DMI, anisotropy, exchange stiffness, and demagnetizing fields compete with each other. All of these energies are also temperature dependent. Chiral spin textures have been put forward for use in some types of magnetic memories, sensors, and computing devices [3]. Many proposed devices use electric current to drive domain walls or skyrmions along narrow magnetic strips. The induced Joule heating will raise the temperature of the devices. Moreover, electronic devices are expected to operate over a range of temperatures around room temperature. It is therefore important to understand the temperature dependence of the different energy contributions. The changes in anisotropy, exchange stiffness, and demagnetizing fields with temperature are reasonably well understood but the DMI less so. It is therefore important to measure the temperature dependence of DMI in a variety of candidate materials to improve understanding.

There is also a fundamental interest because the temperature dependence can lead to a better understanding of the microscopic origin of the DMI in magnetic multilayers. However, there is as yet little agreement between the re-

sults. Anisotropy decreases with increasing temperature in a power law $K_u(T)/K_u(T=0) = m(T)^{l(l+1)/2}$, where $m = M_S(T)/M_S(0)$, the reduced magnetization, and l is the order of the anisotropy. This result is derived from Callen-Callen theory [4,5]. There is not such a simple theory for the temperature dependence of the exchange stiffness or of the DMI, but numerical simulations suggest that they also follow power laws $A(T)/A(T=0) = m(T)^\alpha$ and $D(T)/D(T=0) = m(T)^\delta$ and that the exponents α and δ are the same [6–8]. While these works calculated $\alpha = 1.5$, the important conclusion that should be drawn from them is that $\alpha = \delta$. In general, the value of the exponent will vary depending on the choice of lattice. One experimental study on Pt/Co/Cu superlattices [9] found $D(m) \sim m^{4.9}$, while another on [Pt/CoFeB/Ru]₂ [10] measured $D(m) \sim m^{1.86}$. So far, it is not clear why such different values have been found.

Here, we measure the temperature dependence $D(T)$ of the DMI in Pt/FM/Ir multilayers that are analogs of those in several previous reports in which skyrmions are the focus [11–13]. The ferromagnet (FM) is amorphous CoFeB or CoB, originally chosen to try and avoid the problems of skyrmion pinning at grain boundaries. Pt and Ir are chosen because they are expected to give rise to DMI of opposite signs at the top and bottom interface and thus a large net DMI, although this is disputed [14]. We measure DMI by fitting an expression for the domain wall energy density [15], for which the inputs are temperature-dependent measurements of the saturation magnetization M_S , the exchange stiffness A , the effective perpendicular anisotropy K_{eff} , and the domain period d . The low-temperature exchange stiffness is determined by fitting an expression for Bloch's law in a thin film to

*T.A.Moore@leeds.ac.uk

$M_S(T)$, while the domain period is determined from images of the demagnetized domain pattern obtained by wide-field Kerr microscopy in the temperature range 9–290 K. In the Pt/CoFeB/Ir multilayers that we study, the DMI varies between 1.0 and 1.8 mJ/m², depending on the temperature, while in the Pt/CoB/Ir multilayers, the DMI lies in a narrower range between 0.3 and 0.5 mJ/m². We find that A , K_u , and D all scale close to the theoretically predicted behavior.

II. METHODS

The multilayers that we studied consisted of (i) [Pt(2.3 nm)/Co₆₈Fe₂₂B₁₀(0.7 nm)/Ir(0.5 nm)]_{*n*} (hereafter referred to as CoFeB) and (ii) [Pt(2.3 nm)/Co₆₈B₃₂(0.8 nm)/Ir(0.5 nm)]_{*n*} (CoB) deposited by dc magnetron sputtering on a 3 nm Ta seed layer on a thermally oxidized Si substrate. Thicknesses are nominal values. A 2.3 nm capping layer of Pt was deposited on top to prevent oxidation. The number of repeats n was varied from 1 to 20, and then the samples were subjected to an ac demagnetizing procedure, yielding a maze domain structure at zero field. Three samples were then selected for further study according to their suitability for DMI measurement: those with a large number of domains in the typical field of view in a wide-field Kerr microscope (approximately 200 × 200 μm square) to provide a reasonable statistical estimate of the domain period but with domains that were still well resolved, no narrower than 400 nm. The samples thereby selected were CoFeB ($n = 2$) and CoB ($n = 5$ and 7).

The saturation magnetization was measured from superconducting quantum interference device (SQUID)-vibrating sample magnetometer (VSM) hysteresis loops in the temperature range 9–290 K, and the exchange stiffness at low temperature was found by fitting a modified version of the Bloch $T^{3/2}$ law for thin films to the normalized SQUID-VSM moment vs temperature data.

For thin films, the spin wave spectrum is quantized in the thickness direction which leads to a difference in the temperature dependence of magnetization. Bloch's law can be derived [16,17] in this case by assuming a continuous spin-wave spectrum in plane but a discrete spectrum in the thickness, resulting in the following equation:

$$\frac{M_S(T)}{M_S(0)} = 1 + \frac{k_B T}{8\pi t A(0)} \sum_{p=0}^{N-1} \ln \left[1 - \exp \left(-\frac{g\mu_B}{M_S(0) k_B T} \left\{ M_S(0) B_0 + 2A(0) \left[\frac{p}{(N-1) a_z} \right]^2 \right\} \right) \right], \quad (1)$$

where $M_S(0)$ is the zero temperature magnetization, k_B is the Boltzmann constant, T is the temperature, t is the thickness of a single FM layer, $A(0)$ is the exchange stiffness at low temperature, N is the number of atomic layers in the thickness t , $g = 2.0023$ is the electron g factor, B_0 is an applied field which saturates the magnetization (here, $B_0 = 1.5$ T), and a_z is the distance between atomic layers in the z direction. This differs for different lattice types [simple cubic, body-centered cubic (bcc), face-centered cubic (fcc)] and orientations, but all are based on a cubic lattice parameter $a = 0.355$ nm [18]. As the FM layers are amorphous, the choice of a_z is somewhat

arbitrary; we use values that would correspond to bcc and fcc lattices in the [100] and [111] orientations. Equation (1) implies that $M_S(T)$ does not depend on n , which is indeed what we observe across the range of n .

The value of exchange stiffness in Bloch's law is the zero temperature value. Exchange stiffness decreases with increasing temperature due to renormalization of the magnon spectrum by the thermal magnons [19]. Theory and experiment find an approximate power law scaling of the exchange stiffness with the temperature-dependent magnetization where the exponent depends on the lattice geometry [7]. In our analysis, we use $A(T)/A(0) = A(m) \sim m^{1.8}$, in line with theory [8].

The temperature dependence of the magnetic anisotropy field H_K was measured from in-plane SQUID-VSM hysteresis loops. From this, we calculate the effective perpendicular anisotropy $K_{\text{eff}}(T) = \frac{1}{2} H_K(T) \mu_0 M_S(T)$. The intrinsic perpendicular anisotropy $K_u(T)$ is then calculated by accounting for the shape anisotropy for a thin film $K_{\text{eff}}(T) = K_u(T) - \frac{1}{2} \mu_0 [M_S(T)]^2$, where μ_0 is the vacuum permeability.

In principle, $K_u(T)$ contains both bulk magnetocrystalline anisotropies and interface anisotropies. However, for amorphous transition metal films, we expect the bulk anisotropy to be negligible. The main source of anisotropy is a two-ion anisotropy at the interfaces, for example, Pt-Co, where the spin-orbit coupling of the Pt leads to an anisotropic exchange favoring an out-of-plane orientation for the magnetization. The scaling of two-ion anisotropies according to Callen-Callen theory [4,5] is $K_u \sim m^2$.

We measured the magnetic domain period in the temperature range 9–290 K from images of the demagnetized domain pattern obtained by wide-field Kerr microscopy. We first saturated the samples in sufficient out-of-plane field (30–50 mT) and then demagnetized them at room temperature by applying a sinusoidally varying out-of-plane field at 0.5 Hz decaying over 120 s from a maximum amplitude of 30 mT down to zero. We then mounted each sample in turn in an optical cryostat, cooled to 9 K, and captured an image of the domain pattern at several set temperatures while warming back up to room temperature. Using a similar method to Agrawal *et al.* [20],

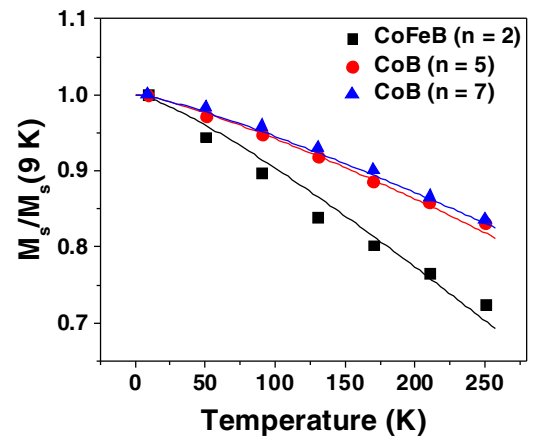


FIG. 1. $M_S(T)$ for [Pt(2.3 nm)/Co₆₈Fe₂₂B₁₀(0.7 nm)/Ir(0.5 nm)]_{*n=2*} and [Pt(2.3 nm)/Co₆₈B₃₂(0.8 nm)/Ir(0.5 nm)]_{*n=5,7*}, normalized to the low-temperature value. The solid lines are fits to the data using Eq. (1)

TABLE I. Extracted low-temperature values of magnetic parameters for the three measured thin films.

	$M_S(9K)$ (MA/m)	$A(9K)$ (pJ/m)	$K_{\text{eff}}(9K)$ (MJ/m ³)	$K_u(9K)$ (MJ/m ³)	$D(9K)$ (mJ/m ²)
CoFeB ($n = 2$)	1.36 ± 0.07	5.5 ± 1.7	1.01 ± 0.08	2.18 ± 0.13	1.8 ± 0.5
CoB ($n = 5$)	1.25 ± 0.04	7.3 ± 1.7	0.80 ± 0.04	1.78 ± 0.08	0.47 ± 0.40
CoB ($n = 7$)	1.26 ± 0.05	7.5 ± 1.8	0.32 ± 0.01	1.32 ± 0.08	0.52 ± 0.31

we extracted the domain period from these images. Briefly, a fast Fourier transform of the image produces rings at a characteristic wavelength related to the maze domains. We extracted this wavelength by radially averaging in reciprocal space and fitting a Gaussian function to the intensity. Transforming back into real space, the peak of the function gave the average domain period d .

III. RESULTS AND DISCUSSION

Figure 1 shows $M_S(T)/M_S(9K)$ for CoFeB ($n = 2$) and CoB ($n = 5$ and 7) thin films. Fitting the data with Eq. (1) yields the low-temperature value of the exchange stiffness A for each sample, given in Table I. There is a considerable uncertainty in the number of atomic layers represented by the thickness of the film because the film is likely to be rough at the interfaces. We therefore estimated the uncertainty in A

by calculating A for $n_z \pm 1$ from the nominal value $n_z = t/a_z$ and taking the largest difference in A as the uncertainty. Our estimated error is therefore large (up to 30%), but we believe it is a realistic estimate of how well A can currently be inferred from thermodynamic measurements in amorphous films. All the values of A here lie within the range of the uncertainty estimated above. We then extrapolated the temperature dependence of A using the power law scaling $A(T)/A(9K) = [M_S(T)/M_S(9K)]^{1.8}$ from theory [8].

Figure 2 shows hysteresis loops measured at room temperature (290 K) using an out-of-plane field [Fig. 2(a)] and in-plane field [Fig. 2(b)]. The former show an expected broadening in the switching field distribution as n increases due to the increase in interface roughness as successive layers are deposited. The latter were measured as a function of temperature to obtain $H_K(T)$ and thus K_{eff} . The low-temperature values of K_{eff} and the intrinsic perpendicular anisotropy K_u are reported in Table I. The uncertainty in the anisotropy is mainly due to the error in measuring the volume of the sample. Figure 3 shows a log-log plot of K_u normalized by the low-temperature value plotted against the normalized magnetization. The slope of the linear fit κ ranges from 1.88 to 2.09 for the different thin films, consistent with a power law scaling of $K_u \sim m^2$ for a two-ion interfacial anisotropy. Table II lists the scaling parameters.

Figure 4 shows typical demagnetized domain patterns at room temperature and the extracted domain period $d(T)$ as a function of the temperature. The domain period does not change with the temperature. For each temperature, we use $d(T)$, $M_S(T)$, $A(T)$, and $K_{\text{eff}}(T)$ and calculate the domain

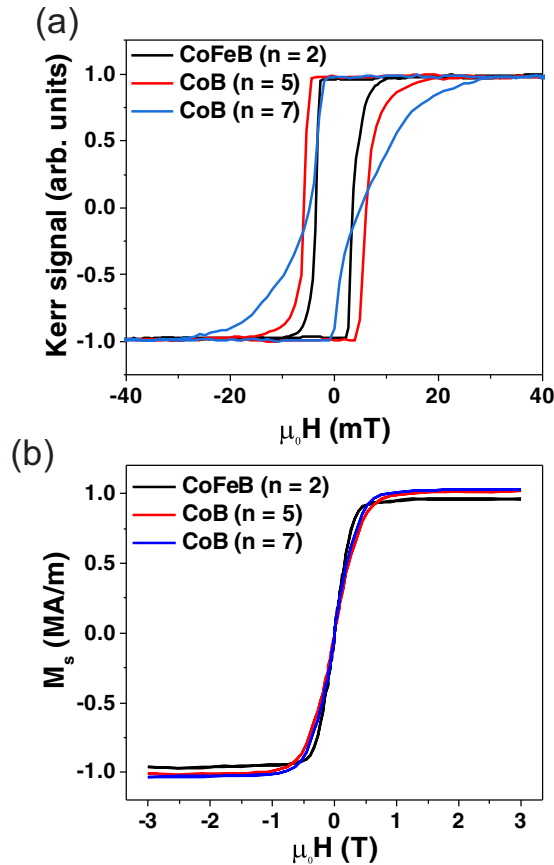


FIG. 2. (a) Hysteresis loops measured at room temperature by magneto-optic Kerr effect with field applied out of plane. (b) Hysteresis loops measured at room temperature by SQUID-VSM with field applied in plane.

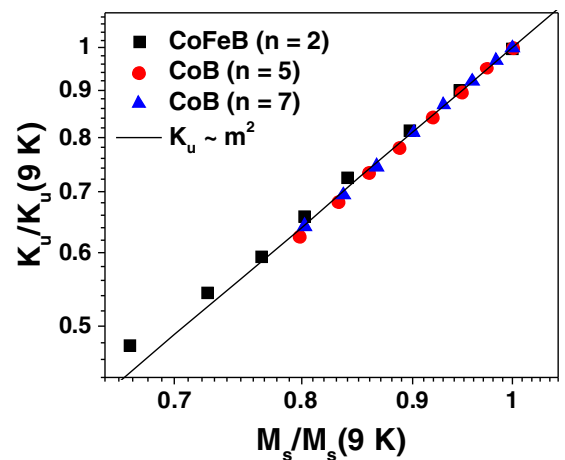


FIG. 3. Log-log plot showing the scaling of the intrinsic perpendicular anisotropy K_u with M_S . The solid line represents the Callen-Callen scaling law $K_u \sim m^2$. Linear fits (not shown) to the data yield the scaling parameters in Table II.

TABLE II. Scaling exponents of the magnetic parameters for the three measured thin films. Asterisk (*) denotes theoretical value.

	α	κ	δ
CoFeB ($n = 2$)	1.8*	1.88 ± 0.03	1.65 ± 0.04
CoB ($n = 5$)	1.8*	2.09 ± 0.02	1.81 ± 0.09
CoB ($n = 7$)	1.8*	2.05 ± 0.02	1.86 ± 0.05

wall energy density (in J/m²) [21]:

$$\sigma_{\text{DW}}(T) = \frac{\mu_0 [M_s(T)]^2 f d(T)^2}{n \tilde{t}} \times \sum_{\substack{k=1 \\ k \text{ odd}}}^{\infty} \frac{1}{(\pi k)^3} \left\{ 1 - \left[1 + \frac{2k\pi n \tilde{t}}{d(T)} \right] \exp \left[\frac{-2k\pi n \tilde{t}}{d(T)} \right] \right\}, \quad (2)$$

where f is the magnetic volume ratio of the full stack, and \tilde{t} is the thickness of one Pt/FM/Ir unit in the uniform medium approximation [15]. Here, $f = 0.2$ or 0.22 , and $\tilde{t} = 3.5$ or 3.6 nm based on the nominal layer thicknesses in the CoFeB and CoB samples, respectively. We find D from the theoretical domain wall energy density [2]:

$$\sigma_{\text{DW}}(T) = 4\sqrt{A(T)K_{\text{eff}}(T)} - \pi |D(T)|. \quad (3)$$

This analysis yields $D(T)$ for each sample [Fig. 5(a)]. The uncertainty in A dominates the uncertainty in D . Here, D for both CoB samples is the same within error, as expected, because the interfaces are the same, and the only difference is the

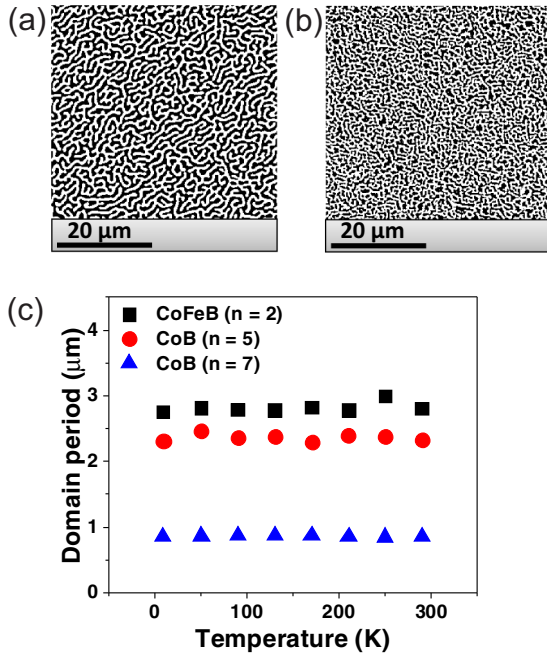


FIG. 4. Demagnetized domain patterns imaged by Kerr microscopy at room temperature for (a) CoFeB ($n = 2$) and (b) CoB ($n = 7$). The images have been adjusted to display maximum contrast between up/down domains. (c) Domain period vs temperature for all three samples. Error bars are smaller than the data points.

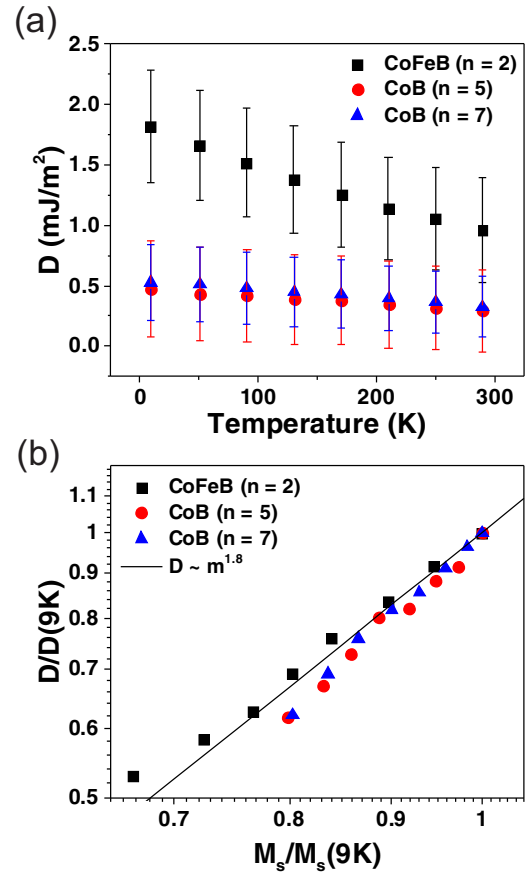


FIG. 5. (a) DMI constant vs temperature for [Pt(2.3 nm)/Co₆₈Fe₂₂B₁₀(0.7 nm)/Ir(0.5 nm)]_{n=2} and [Pt(2.3 nm)/Co₆₈B₃₂(0.8 nm)/Ir(0.5 nm)]_{n=5,7}. (b) Log-log plot showing the scaling of D with M_s , normalized by the low-temperature values. The solid line represents $D \sim m^{1.8}$. Linear fits (not shown) to the data yield the scaling parameters in Table II.

number of repeats n . The DMI of the CoFeB sample is larger than that of the CoB samples (Table I), which we can ascribe to the presence of Fe and also the smaller atomic percentage of B in the CoFeB sample. The DMI in the CoB samples is in the range of what might be expected given a previous measurement in a [Pt(1.0 nm)/Co₈₀B₂₀(0.7 nm)/Ir(1.0 nm)]_{n=6} multilayer [22]. In relative terms, the temperature dependence of the DMI for the CoFeB and CoB samples is the same. Figure 5(b) shows log-log plots of $D(T)$ normalized by the low-temperature value against the normalized magnetization. Linear fits yield the scaling exponents, which range from 1.65 to 1.86 (Table II). The values of the scaling are nearly all the same within error. The scaling for CoFeB ($n = 2$) is only less than that for CoB samples because the data is skewed by one point at room temperature. The scaling parameters are close to the exchange stiffness scaling ~ 1.8 and align with previous predictions and results [10,16]. The similar scaling of A and D explains why the domain period is almost independent of temperature. Furthermore, if different values for the scaling of A are used in the analysis (a reasonable range is 1.5–2.0), the scaling of D is the same within the uncertainty of the measurement, i.e., $\alpha = \delta$, a result consistent with numerical simulations [6–8].

IV. SUMMARY

We have measured the temperature dependence of the magnetization, perpendicular anisotropy, and demagnetized domain period in Pt/CoFeB/Ir and Pt/CoB/Ir multilayers. The domain period does not change significantly as the temperature is varied from 9 to 290 K. This result can only be obtained if A and D have the same temperature dependence, as predicted by theory. Assuming a scaling of $A \sim m^{1.8}$, we find that $D \sim m^{1.8}$, and we report values for the DMI in these films across the temperature range. Pt/CoFeB/Ir exhibits a larger DMI than Pt/CoB/Ir, which we ascribe to the presence of Fe and the smaller at. % of B in the former.

Data associated with this paper are available from the Research Data Leeds repository [23].

ACKNOWLEDGMENTS

K.A. is supported by Jouf University and J.B. by a Royal Society University Research Fellowship. We acknowledge funding from the Engineering and Physical Sciences Research Council (EPSRC) Grants No. EP/T006803/1 and No. EP/T034343/1. We also acknowledge the Exeter Time-Resolved Magnetism Facility (EPSRC Grant Reference EP/R008809/1) for variable-temperature, wide-field Kerr microscopy.

-
- [1] A. Fert and P. M. Levy, Role of Anisotropic Exchange Interactions in Determining the Properties of Spin-Glasses, *Phys. Rev. Lett.* **44**, 1538 (1980).
- [2] A. Thiaville, S. Rohart, É. Jué, V. Cros, and A. Fert, Dynamics of Dzyaloshinskii domain walls in ultrathin magnetic films, *Europhys. Lett.* **100**, 57002 (2012).
- [3] K. Everschor-Sitte, J. Masell, R. M. Reeve, and M. Kläui, Perspective: Magnetic skyrmions—overview of recent progress in an active research field, *J. Appl. Phys.* **124**, 240901 (2018).
- [4] H. B. Callen and E. Callen, The present status of the temperature dependence of magnetocrystalline anisotropy, and the $l(l+1)/2$ power law, *J. Phys. Chem. Solids* **27**, 1271 (1966).
- [5] E. C. Callen and H. B. Callen, Magnetostriction, forced magnetostriction, and anomalous thermal expansion in ferromagnets, *Phys. Rev.* **139**, A455 (1965).
- [6] U. Atxitia, D. Hinzke, O. Chubykalo-Fesenko, U. Nowak, H. Kachkachi, O. N. Mryasov, R. F. Evans, and R. W. Chantrell, Multiscale modeling of magnetic materials: temperature dependence of the exchange stiffness, *Phys. Rev. B* **82**, 134440 (2010).
- [7] R. Bastardis, U. Atxitia, O. Chubykalo-Fesenko, and H. Kachkachi, Unified decoupling scheme for exchange and anisotropy contributions and temperature-dependent spectral properties of anisotropic spin systems, *Phys. Rev. B* **86**, 094415 (2012).
- [8] R. Moreno, R. F. L. Evans, S. Khmelevskyi, M. C. Muñoz, R. W. Chantrell, and O. Chubykalo-Fesenko, Temperature-dependent exchange stiffness and domain wall width in Co, *Phys. Rev. B* **94**, 104433 (2016).
- [9] S. Schlotter, P. Agrawal, and G. S. D. Beach, Temperature dependence of the Dzyaloshinskii-Moriya interaction in Pt/Co/Cu thin film heterostructures, *Appl. Phys. Lett.* **113**, 092402 (2018).
- [10] Y. Zhou, R. Mansell, S. Valencia, F. Kronast, and S. van Dijken, Temperature dependence of the Dzyaloshinskii-Moriya interaction in ultrathin films, *Phys. Rev. B* **101**, 054433 (2020).
- [11] C. Moreau-Luchaire, C. Moutafis, N. Reyren, J. Sampaio, C. A. F. Vaz, N. Van Horne, K. Bouzehouane, K. Garcia, C. Deranlot, P. Warnicke, P. Wohlhüter, J.-M. George, M. Weigand, J. Raabe, V. Cros, and A. Fert, Additive interfacial chiral interaction in multilayers for stabilization of small individual skyrmions at room temperature, *Nat. Nanotechnol.* **11**, 444 (2016).
- [12] K. Zeissler, S. Finizio, K. Shahbazi, J. Massey, F. Al Ma’Mari, D. M. Bracher, A. Kleibert, M. C. Rosamond, E. H. Linfield, T. A. Moore, J. Raabe, G. Burnell, and C. H. Marrows, Discrete Hall resistivity contribution from Néel skyrmions in multilayer nanodiscs, *Nat. Nanotechnol.* **13**, 1161 (2018).
- [13] K. Zeissler, S. Finizio, C. Barton, A. J. Huxtable, J. Massey, J. Raabe, A. V. Sadovnikov, S. A. Nikitov, R. Brearton, T. Hesjedal, G. van der Laan, M. C. Rosamond, E. H. Linfield, G. Burnell, and C. H. Marrows, Diameter-independent skyrmion Hall angle observed in chiral magnetic multilayers, *Nat. Commun.* **11**, 428 (2020).
- [14] K. Shahbazi, J.-V. Kim, H. T. Nembach, J. M. Shaw, A. Bischof, M. D. Rossell, V. Jeudy, T. A. Moore, and C. H. Marrows, Domain-wall motion and interfacial Dzyaloshinskii-Moriya interactions in Pt/Co/Ir(t_{Ir})/Ta multilayers, *Phys. Rev. B* **99**, 094409 (2019).
- [15] S. Woo, K. Litzius, B. Krüger, M.-Y. Im, L. Caretta, K. Richter, M. Mann, A. Krone, R. M. Reeve, M. Weigand, P. Agrawal, I. Lemesch, M.-A. Mawass, P. Fischer, M. Kläui, and G. S. D. Beach, Observation of room-temperature magnetic skyrmions and their current-driven dynamics in ultrathin metallic ferromagnets, *Nat. Mater.* **15**, 501 (2016).
- [16] H. T. Nembach, J. M. Shaw, M. Weiler, E. Jué, and T. J. Silva, Linear relation between Heisenberg exchange and interfacial Dzyaloshinskii-Moriya interaction in metal films, *Nat. Phys.* **11**, 825 (2015).
- [17] J. B. Mohammadi, B. Kardasz, G. Wolf, Y. Chen, M. Pinarbasi, and A. D. Kent, Reduced exchange interactions in magnetic tunnel junction free layers with insertion layers, *ACS Appl. Electron. Mater.* **1**, 2025 (2019).
- [18] K. Zeissler, M. Mruczkiewicz, S. Finizio, J. Raabe, P. M. Shepley, A. V. Sadovnikov, S. A. Nikitov, K. Fallon, S. McFadzean, S. McVitie, T. A. Moore, G. Burnell, and C. H. Marrows, Pinning and hysteresis in the field dependent diameter evolution of skyrmions in Pt/Co/Ir superlattice stacks, *Sci. Rep.* **7**, 15125 (2017).
- [19] C. Kittel, *Quantum Theory of Solids*, 2nd ed. (John Wiley & Sons, New York, 1987).
- [20] P. Agrawal, F. Büttner, I. Lemesch, S. Schlotter, and G. S. D. Beach, Measurement of interfacial Dzyaloshinskii-Moriya

- interaction from static domain imaging, *Phys. Rev. B* **100**, 104430 (2019).
- [21] I. Lemesh, F. Büttner, and G. S. D. Beach, Accurate model of the stripe domain phase of perpendicularly magnetized multilayers, *Phys. Rev. B* **95**, 174423 (2017).
- [22] J. Lucassen, M. J. Meijer, O. Kurnosikov, H. J. M. Swagten, B. Koopmans, R. Lavrijsen, F. Kloedt-Twesten, R. Frömter, and R. A. Duine, Tuning Magnetic Chirality by Dipolar Interactions, *Phys. Rev. Lett.* **123**, 157201 (2019).
- [23] <https://doi.org/10.5518/1071>